ARCTIC OFFSHORE ENGINEERING

Appendix II. - Statistical Size Effect

The decrease of observed nominal strength with the size of specimen has usually been explained statistically. The strength value is assumed to vary randomly throughout the material, and so in a specimen of a larger size the chance of encountering a smaller minimum strength is higher. The size effect law obtained in this manner then depends on the assumed statistics of strength distribution, or the statistics of the size of microscopic flaws which cause the local strength reduction. This classical, statistical approach has, however, several significant differences from the present size effect law.

One difference is due to the fact that for volumes larger than a certain characteristic volume the chance of encountering a still smaller strength (or a still larger flaw) does not increase. In such a case the statistically based size effect reaches an asymptotic value at a certain specimen size, and does not decrease any more for larger specimen sizes. On the other hand, the present size effect law continues decreasing.

Another, more significant difference is due to the fact that the amount of energy released from the uncracked part of the structure into the fracturing region is very important. Thus, the same specimen supported rigidly or elastically would have the same strength according to the statistical theory, while according to the present energy-based size effect law the elastically supported specimen can have a much smaller strength. Obviously, a similar phenomenon arises from the geometry of the structure, in the various possible manners the geometry of the uncracked regions of the structure can significantly affect the failure.

Some statistical size effect surely exists, but it may be much less significant than the present energy-based size effect. At least for concrete it seems at the present that all the known size effect can be adequately explained by the energy-based size effect law, although statistically-based theories have previously been offered to provide an explanation.

SEA ICE INDENTATION ACCOUNTING FOR STRAIN-RATE VARIATION

Seng-Kiong Ting[1] and S. Shyam Sunder[2], A.M., A.S.C.E.

ABSTRACT: Global and local indentation pressures in the creeping mode of sea ice deformation are obtained, accounting for the spatial variation of strain-rates. Two approximate methods of analysis are considered; the upper bound and strain path methods. Theoretically postulated velocity fields required in the analysis are calibrated with field measurements. Sea ice behavior is described by a multi-axial power-law creep model and by the multi-axial extension of a new uniaxial model which accounts for both hardening and softening behavior. Results are compared with previously published indentation formulas.

INTRODUCTION

Two levels of ice loading are typically considered in the design of drilling and production platforms for the Arctic. Global ice pressures govern the overall structural geometry and dimensions as well as the foundation design, while local pressures are likely to dictate wall thicknesses and local framing, and may well govern structural cost. Most of the emphasis on ice force research has been on predicting global forces. Only during recent years, as the focus changed from overall feasibility to preliminary and detailed design, has the importance of local pressures emerged. Peak local pressures may be as high as three times the average global pressure. It is widely recognized that uncertainties exist in ice load prediction models in use today and that in some cases design loads may be overestimated by an order of magnitude.

Uncertainties in existing ice load models arise primarily from four sources: (i) incomplete modeling of the thermomechanical behavior of sea ice, (ii) use of semi-empirical formulations, calibrated without adequate regard for similitude modeling and scale effects, (iii) failure to realistically model the contact forces at the ice-structure interface and the presence of macrocracks, and (iv) not accounting for the finiteness of the environmental forces driving the ice features. Both approximate analytical methods and more rigorous numerical models based on the finite and boundary element methods of analysis can be used to study ice-structure interaction at full scale with realistic models for material and interface behavior.

This paper employs two approximate methods of analysis, the upper bound and strain path methods, to study the problem of sea ice indentation in the creeping mode of deformation, accounting for the spatial variation of strain-rates. This is a problem of concern for artificial islands in the Arctic nearshore region, where "break-out" and/or steady indentation conditions occurring in the winter form a basis for select-

[1]Research Assistant, Department of Civil Engineering, Massachusetts Institute of Technology, Cambridge, MA 02139
[2]Assistant Professor of Civil Engineering, Massachusetts Institute of Technology, Room 1-274, Cambridge, MA 02139

ing design ice loads. The key difference in the two analyses is that point stresses within the continuum can be obtained with the strain path method. As a result, local stresses at the ice-structure interface can be estimated, unlike the upper bound method which only yields the global pressure. However, both methods rely on an adequate specification of the velocity field in the ice sheet. This is obtained through a combination of theoretical modeling based on fluid mechanics and field ice movement survey data from an artificial island in the Beaufort Sea. In particular, two theoretical kinematic models are considered: one resulting from the superposition of a point source and a uniform flow (Kinematic Model A) that has been studied previously (3,9); and the other from the superposition of a doublet and a uniform flow (Kinematic Model B).

An important aspect of the analysis is the specification of the mechanical behavior of sea ice. In order to provide continuity with previous work, the isotropic, incompressible three-dimensional extension of the uniaxial power-law creep model is studied. The predicted global ice pressures are compared with those from previously published formulas (1,8). Finally, a new uniaxial law that models the stress-strain-strainrate behavior of sea ice, including its strain-softening behavior, is presented. The strength-strainrate relationship derived from this new model is used to predict global ice pressures during indentation.

BOUND METHOD VERSUS STRAIN PATH METHOD

An upper bound (conservative) solution to a continuum mechanics problem may be derived by relaxing the statical field equations and boundary conditions, and using velocity fields that satisfy the kinematic constraints for the problem. Applying the principle of virtual work and Drucker's convexity criterion, the upper bound estimate of the global load for incompressible materials may be obtained with (4):

$$\int_V S_{ij}^* \dot{\epsilon}_{ij}^* \, dv \geq \int_{S_T} T_i U_i^* \, dS + \int_{S_U} T_i U_i \, dS \qquad (1)$$

where S_{ij}^*, $\dot{\epsilon}_{ij}^*$ and U_i^* are the deviatoric stresses, strain-rates and velocities obtained from an assumed kinematically admissible velocity field. T_i and U_i are the actual surface tractions and velocities.

The upper bound method does not make use of the field equilibrium equations. As such, point stresses in the continuum are unknown. Hill (5) has suggested an approximate method by which octahedral (hydro-static) stresses can be derived from deviatoric stress gradients using the equilibrium equation. This idea was developed and first applied to deep penetration problems in soil mechanics by Baligh (2), who called it the strain path method.

In applying the strain path method to the ice indentation problem, the major assumption is that the strain and strain-rate field can be obtained from the kinematic conditions with no reference to constitutive relations, equilibrium equations, or statical boundary conditions. This is an approximation and hence the derived stress field is approximate in general. However, the method is computationally very attractive when compared with a detailed finite element analysis. In addition, the method provides valuable insights to the indentation problem which is difficult to obtain from a purely numerical approach.

KINEMATIC MODELING OF ICE SHEET

Theoretical Kinematic Models.-- Kinematic Model A is shown in Fig. 1. The streamline passing through the stagnation point defines the bluff-body, i.e., the region where the oncoming sheet of ice cannot enter. The streamfunction, ψ, and flow velocities, U_r and U_θ, follow from the theory of fluid mechanics and are given by:

$$\psi = -U_0 r \sin\theta - U_0 a \theta \qquad (2)$$

$$U_r = \frac{-1}{r}\frac{\partial\psi}{\partial\theta} = U_0 \cos\theta + U_0 \frac{a}{r} \qquad (3)$$

$$U_\theta = \frac{\partial\psi}{\partial r} = -U_0 \sin\theta \qquad (4)$$

where U_0 is the uniform far field velocity. The bluff-body is described by $r=a(\pi-\theta)/\sin\theta$ with the half-width of the body at $r=\infty$ equal to πa. This model assumes that the normal velocity at the ice/bluff-body interface is zero. Even if this is valid, the tangential contact between the moving ice sheet and the half-body could in general be either friction-free or possess finite frictional forces. This imposes a statical boundary condition with which the chosen velocity field may or may not be consistent.

Kinematic Model B is shown in Fig. 2. The bluff-body in this case is a circle of radius, a. This represents flow past a cylindrical indenter with contact at all points on the circumference. The stream-function and flow velocities are given by:

$$\psi = -U_0 r \sin\theta + U_0 \frac{a^2}{r} \sin\theta \qquad (5)$$

$$U_r = U_0 [1 - \frac{a^2}{r^2}] \cos\theta \qquad (6)$$

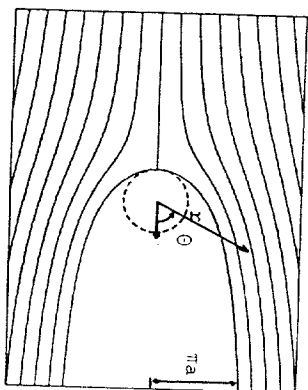$$U_\theta = -U_0 [1 + \frac{a^2}{r^2}] \sin\theta \qquad (7)$$
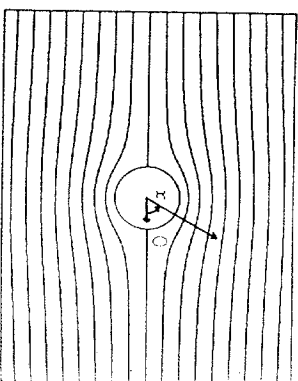
Fig. 1.--Kinematic Model A

Fig. 2.--Kinematic Model B

Calibration with Field Ice Movement Data.-- The theoretical velocity fields are calibrated with field ice movement data from an artificial island in the Beaufort Sea, obtained over a period of seven weeks during peak winter ice formation. The surveys were carried out at the 39 stations at least once per day, although during high movement events th...

surveys were made every 12 hours. The calibration is based on the following three criteria: (a) streamfunction values for a particle at the start and end of the observation period should be equal under steady flow conditions; (b) the average movement rate measured should be approximately equal to the average of the predicted velocities over the observation period; and (c) the measured direction of movement must equal the predicted bearing.

A careful analysis of the data shows that the ice movements downstream and directly at the back of the indenter are of the same order of magnitude as on the upstream side prior to macrocracking, which was observed to occur in a direction perpendicular to the flow on the downstream side. Thus Kinematic Model A which considers no flow within the bluff-body cannot model field conditions prior to macrocracking. Nevertheless, both kinematic models predict relatively accurate streamfunction values over their respective domains of applicability. For Model A the errors vary from less than 1% to as much as 25%, even when there is no macrocrack formation. For Model B, the errors are generally less than 1% in all cases except the case with macrocrack formation. The errors in velocity predictions are much higher for both models. Some stations near the rubble pile surrounding the structure are significantly in error due to an inadequate modeling of the structural geometry, e.g., choice of diameter D. In the cases affected by macrocracking: (a) separate and large regions of the continuum are adequately modeled by both velocity fields, (b) Model B is in general better than Model A. Typical errors in the velocity are on the order of 5% to 10% if the above exceptions are taken into account. The errors in bearing predictions are on the order of 5 to 10 degrees for Kinematic Model B and larger for Model A. The discrepancies, where they are larger, can be explained with arguments similar to that for velocities.

In summary: (a) Kinematic Model A does not adequately model the field data considered here; (b) Kinematic Model B provides a good description of the measured flow field and can be used to explain the observed macrocracking if tensile stresses develop on the downstream side; (c) even after macrocracking, Model B accurately models the upstream flow field; and (d) the transition from creeping behavior to macrocracking occurs for velocities less than 1 ft/hr (85x10-6 m s-1).

ICE PRESSURES FOR POWER-LAW CREEP MODEL

The isotropic, incompressible three-dimensional extension of the uniaxial power-law creep leads to the following constitutive model:

$$S_{ij} = \frac{2}{3}\left(\frac{\sigma_o}{\dot{\varepsilon}_o}\right)^{\frac{1}{N}} \dot{\varepsilon}_e^{\frac{1}{N}-1} \dot{\varepsilon}_{ij} \tag{8}$$

where S_{ij} and $\dot{\varepsilon}_{ij}$ are the deviatoric stress and strain-rate tensors, respectively. The effective strain-rate is defined as:

$$\dot{\varepsilon}_e = \left[\frac{2}{3}\dot{\varepsilon}_{ij}\dot{\varepsilon}_{ij}\right]^{1/2} \tag{9}$$

N is the power-law exponent; σ_o and $\dot{\varepsilon}_o$ are material constants derivable from uniaxial testing of ice. The results presented in this paper are based on the sea ice data of Wang (10).

The basic steps for evaluating stresses using the strain path method are: (a) compute the strain-rate field by differentiating the veloci-

ties with respect to the spatial coordinates, (b) evaluate the deviatoric stress field using the constitutive equations, (c) obtain octahedral stresses by spatially integrating the equilibrium equations, and (d) estimat[e] the total stresses by summing the deviatoric and octahedral stresses.

Then, the local stresses at the ice-structure interface can be obtained from the total stress field, while global pressures may be estimated with the bound method and/or by integration of the local stress field.

The degree of approximation in the estimated stress field can be assessed by comparing the octahedral stresses obtained by integration along different (i.e., orthogonal) paths and by noting the error in satisfying statical boundary conditions. Another way of making the former comparison is to integrate along one path and to compare the magnitude of fictitous body forces required for equilibrium in the orthogonal direction with the stress gradients in that direction.

Ice Pressure Prediction.-- Results from the application of the upper bound and strain path methods of analysis to the chosen kinematic models are presented below.

1. Kinematic Model A: The octahedral stress field for this kinematic model is path independent and as such equilibrium is exactly satisfied. In spite of this, the statical interface boundary conditions may not be satisfied by the model. In addition, the following comments can be made:

(i) the maximum strain-rate occurs at the ice/bluff-body interface at r=a, and is equal to U_o/a;
(ii) the stress field decays as r-2/N, which for N=4 is $1/\sqrt{r}$;
(iii) the stress field is axisymmetric, and
(iv) the octahedral stress is zero for a viscoelastic material (N=1).

The global pressure can be estimated by the upper bound method, assuming a frictionless ice/bluff-body interface. This is similar to the case studied by Bruen and Vivatrat (3), and Eq. (1) reduces to:

$$\frac{P}{2at} \le \frac{N}{\sqrt{3}} \int_0^\pi \left(\frac{\sin\theta}{\theta}\right)^{2N/N} d\theta \sqrt{\frac{2}{5}}\, \dot{\varepsilon}_o \left(\frac{U_o}{a}\right)^{\frac{1}{N}} \tag{9}$$

A second approach to estimating the global pressure involves integration of the local stresses around the bluff-body, i.e.,

$$P = t \int (\sigma_{rr} \cos\theta\, rd\theta + \sigma_{\theta\theta} \sin\theta\, dr) \tag{10}$$

Using the equation for the bluff-body, Eq. (10) shows that P=0, unlike the upper bound method. If the frictional forces predicted by the strain path method at the ice/bluff-body interface are included in the upper bound method, that method also predicts zero pressure. However, the bound theorems do not apply for the case of friction with relative motion. The implications of this finding are more fully discussed for Kinematic Model B.

2. Kinematic Model B: The octahedral stresses for this kinematic model are path dependent, although for N=1 and N=3 the fictitious body force is zero and equilibrium is satisfied exactly. However, the statical interface boundary conditions will in general not be satisfied. In addition, the following comments can be made:

(i) the maximum strain-rate occurs at the ice-structure interface, r=a, and is equal to $2U_o/a$ or $4U_o/D$,

(11) the stress field decays as $r^{-3/N}$ (not $r^{-2/N}$ as predicted by Kinematic Model A), which for N=4 is $r^{-3/4}$,

(iii) the octahedral stress is not axisymmetric, and

(iv) the stress field is zero for a viscoelastic material.

The radial stresses downstream of the indenter are tensile and equal in magnitude to the upstream compressive stresses, consistent with the material law. The tangential stresses behave similarly for typical values of N, although their magnitudes could be less than half of the radial stresses. These are principal stresses at θ=0. As such, it is reasonable to expect a macrocrack formation on the downstream side of the indenter. This is indeed borne out by the field ice movement data.

The global pressure can be estimated using the bound method, assuming either a frictionless interface or an interface with frictional stresses predicted by the strain path method. (The method does not strictly apply for the latter case.) The respective expressions, derived from Eq. (1) for D=2a, are:

No friction

$$\frac{P}{Dt} < \frac{4\pi}{\sqrt{3}} \frac{N}{N+3} \left[\frac{4}{\sqrt{3}} \frac{\sigma_o}{\dot\epsilon_o} \frac{2U_o}{D} \right]^{\frac{1}{N}}$$

With friction

$$\frac{P}{Dt} < \sqrt{3}\pi \frac{N-1}{N+3} \left[\frac{4}{\sqrt{3}} \frac{\sigma_o}{\dot\epsilon_o} \frac{2U_o}{D} \right]^{\frac{1}{N}}$$ (11)

(12)

The ratio of Eq. (11) to Eq. (12) is 4N/3(N-1), which varies between 1.8 and 2.2 for 2.5≤N≤4. Intuitively, interface friction should increase indentation pressures. However, both Kinematic friction models studied here predict a significant decrease in pressure. This is because they are derived from considerations for ideal, non-viscous fluids and as such do not correctly model interface conditions. Even if more exact velocity fields can be postulated theoretically, the available field data does not provide adequate resolution of the ice movements in the immediate vicinity of the structure to calibrate the kinematic models.

Integration of the local stresses around the bluff-body yields another estimate of global pressure accounting for the frictional stresses of the strain path method:

$$\frac{P}{Dt} = \frac{\pi}{2\sqrt{3}} (N-1) \left[\frac{4}{\sqrt{3}} \frac{\sigma_o}{\dot\epsilon_o} \frac{2U_o}{D} \right]^{\frac{1}{N}}$$ (13)

Both Eqs. (12) and (13) predict zero pressure for a viscoelastic material. Furthermore, the ratio of the upper bound method to Eq. (13) is 6/(N+3), which varies between 0.86 and 1.09 for 2.5<N<4.

For the artificial island considered in this paper the maximum strain-rate just prior to macrocracking is on the order of 10^{-6} s^{-1} or less. The peak local tangential stresses are on the order of 80 psi (0.55 MPa), the peak local radial stresses are on the order of 320 psi (2.2 MPa). The radial stresses are compressive upstream of the indenter and tensile on the downstream side, and are distributed in a cosinusoidal fashion. The typical order of magnitude value for the global pressure is about 350 psi (2.4 MPa). A key inference here is that the local and global pressures are on the same order of magnitude. If instead Eq. (11) is used to estimate the global pressure, the peak local pressure becomes approximately half the global pressure.

Table 1.--Comparison of Average Global Pressures for Power-Law Creep with N=4 and Average Strain-Rate of $U_o/2D$

Model	Constraints	φ
API	Plane Strain	4.12
	Plane Stress	3.13
Ponter et al. (1983)	Plane Strain	3.64
	Plane Stress	1.85
Model A	D = 2πa	3.22
	D = 2a	7.60
Model B		7.22

Comparison with Other Ice Pressure Formulas.-- Average global pressures during sea ice indentation can be estimated using any one of the many predictive models available in the literature. In this study, the global pressures predicted by Kinematic Models A and B, neglecting the comparison of interface frictional stresses, are compared with the models of API (1) and Ponter et al. (8). The general form of all these models is given by:

$$\frac{P}{Dt} = \phi \, \sigma(\dot\epsilon_a)$$ (14)

where φ is a constant depending in general on N, and $\sigma(\dot\epsilon_a)$ is the uniaxial strength of ice evaluated at some average strain-rate, $\dot\epsilon_a = U_o/(\phi\Psi D)$ with Ψ being a second constant. In order to compare the various formulations, $\phi\Psi$ is assumed equal to two as suggested by API (1) and the comparison can therefore be based on the parameter φ.

The values of φ predicted by the four formulations for a power-law creep model with N=4 is given in Table 1. At first glance the numbers seem highly scattered, varying from 1.85 to 7.60. However, there are important differences among the models. The first two formulations apply for a flat indenter with ice pressures being allowed to develop only on the upstream side. For the API model, the sea ice is assumed columnar and the contact factor is set to one. In Ponter et al.'s model, a correction factor of 1.1 is applied to φ to make results consistent with Kinematic Model A, the problem geometry (Fig. 1) is different from the other models and the choice of indenter diameter is subjective. If the indenter diameter is chosen as 2πa, φ is about 42% of that for D=2a. In the former case the indenter is located far away (r→∞) from the tip of the bluff-body with the region in between consisting of inert ice, while in the latter case the indenter is located at the tip of the bluff-body with the inert region downstream of the indenter. Field data on deformation patterns considered here indicate that both assumptions may be unrealistic. The φ factor for Model B is based on a circular indenter with compressive and tensile stresses on the upstream and downstream sides respectively. This is more representative of actual field conditions prior to breakout.

If the API and Ponter et al. models are extended to account for downstream tensile stresses, the φ factors would probably be twice as much since for the problem and material model considered (a) tensile and compressive strengths are equal, and (b) stress levels are equal but opposite in sign on the upstream and downstream sides. Then, φ for the

API model would vary between 6.3 and 8.2 while for Ponter et al.'s it would vary between 3.7 and 7.3. For the artificial island considered earlier and other typical artificial islands with $D/t \geq 20$, the behavior is closer to a plane stress condition. Both Model B and the API model tend to predict similar global pressures under this scenario.

ICE PRESSURES FOR NEW UNIAXIAL MODEL

The uniaxial behavior of sea ice has often been idealized with the power-law creep formulation. This model relates the strength of ice to the strain-rate, and as such is an incomplete description of the stress-strain-strainrate characteristics of the material. Several investi-gators have proposed more complete uniaxial models, some empirical in nature, that seem to be able to reproduce the post-peak decrease of stress in ice under constant strain-rate conditions. However, most of these models have not been fit to any specific data on sea ice. In addition, since they represent behavior only under constant strain-rate conditions, it is difficult to extend the models to other loading conditions such as constant stress (creep) and stress-rates.

A phenomenological approach based on simple thermorheological models is used here to develop a new uniaxial model, which is then calibrated with the sea ice data of Wang (10). This model applies equally well for constant stress-rate and creep conditions. In addition, under constant strain-rate conditions the strain at peak stress is a function of the strain-rate. The strength-strainrate relationship derived from the new uniaxial model is extended for multi-axial stress states and then applied to obtain indentation pressures.

New Uniaxial Constitutive Model.-- The new uniaxial constitutive model is based on the concept that the strength of an ice specimen is affected simultaneously by work or strain hardening and work softening or recovery. The latter phenomenon may occur due to recrystallization or micro-voids formation. This concept was used by Orowan (7) for examining steady state creep, and may be expressed as:

$$\frac{d\sigma}{dt} = \frac{\partial \sigma}{\partial \varepsilon} \, \dot{\varepsilon} + \frac{\partial \sigma}{\partial t}$$

(15)

where $h = \partial \sigma / \partial \varepsilon$ is the coefficient of work hardening and $r = -\partial \sigma / \partial t$ is the rate of recovery. The parameter h is generally modelled as (6):

$$h = A \, \dot{\varepsilon}^{1/N} \exp\,(-M\varepsilon)$$

(16)

where Q is the activation energy and R is the universal gas constant; A, N and M are the parameters of the equation. Due to a lack of general models for work softening, it is assumed here that the form is similar to that for work hardening:

$$r = B \, \dot{\varepsilon}^{1/K} \exp\,(-L\varepsilon)$$

(17)

with B, K and L being the parameters of the equation. Substituting Eqs. (16) and (17) into Eq. (15) yields after integration (assuming $\dot{\varepsilon}$ and τ are constant with $\varepsilon = \dot{\varepsilon} t$ and $\sigma = 0$ at $t=0$):

$$\sigma = \left[\frac{A}{M} \, \dot{\varepsilon}^{1/N}\left[1 - \exp\,(-M\varepsilon)\right] - \frac{B}{L} \, \dot{\varepsilon}^{1/K-1}\left[1 - \exp\,(-L\dot{\varepsilon})\right] \right]$$
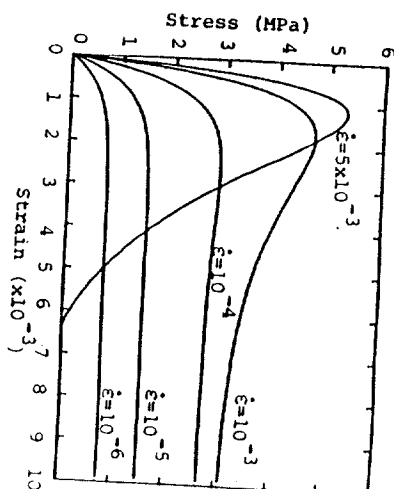
(18)

Fig. 3.--Stress-Strain Curves for Constant Strain-Rate Using New Model

The parameters of Eq. (18) obtained from Wang's (10) experimental data are: $A=114025$ MPa $s^{1/3}$, $B=217408$ MPa $s^{2/3}$, $M=1411.2$, $L=430$, $N=3$ and $K=0.6$. The stress-strain plots for the new model are shown in Fig. 3.

The two plots of the stress-strain behavior for $\dot{\varepsilon}=10^{-3}$ s^{-1} shown in Ref. 10 are vastly different, one shows strain softening behavior with zero residual strength, while in the other the stress reduces to very sharply for strains exceeding the peak stress. The new model (Fig. 3) reflects this behavior for strain-rates of $10^{-2} - 10^{-3}$ s^{-1}, suggesting that the stress-strain behavior is very sensitive to strain-rate in this region.

Ice Pressure Prediction.-- The uniaxial model developed here relates the stress to strain and strain-rate. The strength-strainrate relation-ship derived from the model is extended for multi-axial stress states under the assumptions of isotropy and incompressibility made earlier for the power-law creep model. These assumptions are reasonable for the strain-rates of interest in this paper. Ice pressures obtained with this model can then be compared with the results for the power-law creep model. A general analysis strategy to incorporate the effect of strain and temperature is currently under development.

The strength-strainrate relationship for the new uniaxial model is plotted in Fig. 4 and compared with the power-law creep model. Notice that the new model predicts lower strength at strain-rates less than 10^{-5} s^{-1}, consistent with experimental data which suggests that the effective power-law exponent is an increasing function of strain-rate.

The new constitutive model can be viewed as the superposition of three power-law models of the type considered in the previous section and as such the local pressures will be distributed similarly. A typical order of magnitude global pressure for the artificial island considered here, based on Kinematic Model B and Eq. (13), is about 250 psi (1.7 MPa). This is only 70% of the pressure predicted by the power-law creep model. The 30% reduction in pressure is significant, although this reduces to approximately 10% when using Eq. (11). The pressure in the latter case is about 480 psi (3.3 MPa).
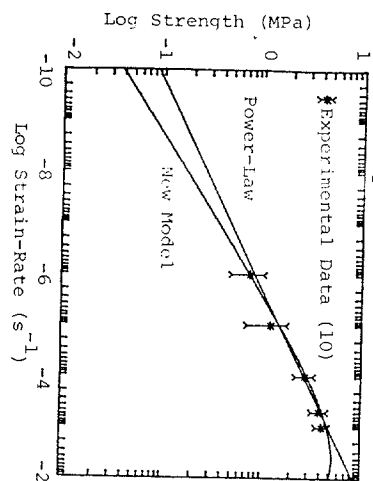
Fig. 4.--Comparison of Uniaxial Strength-Strainrate Relations

CONCLUSIONS

This study of global and local indentation pressures in the creeping mode of sea ice deformation, accounting for the spatial variation of strain-rates, leads to the following specific conclusions:

1. Kinematic Model B better models the ice movement survey data obtained from an artificial island in the Beaufort Sea than Kinematic Model A.

2. In the creeping mode of ice deformation, the local ice pressures are of the same order of magnitude as or lower than the global pressures. Even if the global pressures are reduced, e.g., by a factor of three, to account for scale (fracturing) effects, the local pressures based on the strain path method will only be 1.5 (and not three) times the upper bound global pressure neglecting interface friction.

3. Under essentially plane stress conditions, Kinematic Model B and the API model (11) predict similar global pressures. For a typical artificial island just prior to break-out with ice movements of less than 1 ft/hr (85x10-6 m s^-1), Model B predicts a pressure (neglecting interface friction) of approximately 530 psi (3.7 MPa).

4. The constitutive law based on the new uniaxial model predicts global pressures that are lower than that from the power-law creep model. For a typical artificial island, this reduction can be as much as 10-30 percent.

A key finding of this work is that for the rate-dependent material models describing sea ice behavior, interface adfreeze and friction stresses may significantly influence both local and global ice pressures. This has major economic consequences for platform design. Incorporation of these "non-conservative" stresses within the bound method may yield more accurate global ice pressures, but the solutions will not necessarily be upper bounds. More exact estimates of both local and global ice pressures using the strain path method may be

obtained by postulating kinematic models that more correctly model the interface conditions. However, currently available field data does not provide adequate resolution of the ice movements in the immediate vicinity of the structure to calibrate such models. In conclusion, it appears that the development of numerical models based on the finite and boundary element methods of analysis is necessary for more realistically studying ice-structure interaction problems where both global and local pressures are of interest.

ACKNOWLEDGEMENTS

APPENDIX.--REFERENCES

1. API Bulletin on Planning, Designing, and Constructing Fixed Offshore Structures in Ice Environments, Bul. 2N, First Edition, January, 1982.

2. Baligh, M.M., "The Strain Path Method in Geotechnical Engineering," Research Report R84-01, No. 761, Department of Civil Engineering, Massachusetts Institute of Technology, Cambridge, Massachusetts, 1984, 55p.

3. Bruen, F.J., and Vivatrat, V., "Ice Force Prediction Based on Strain-Rate Field," Third International Symposium on Offshore Mechanics and Arctic Engineering, New Orleans, LA, February 12-16, 1984, 7p.

4. Hill, R., "The Mathematical Theory of Plasticity," Oxford University Press, London, 1950, 355 p.

5. Hill, R., "A General Method of Analysis for Metal-Working Process," Journal of the Mechanics and Physics of Solids, Vol. 11, 1963, pp. 305-326.

6. Meyers, M.A. and Chawla, K.K., "Mechanical Metallurgy - Principles and Applications," Prentice-Hall Inc., Englewood Cliffs, New Jersey, 1984, 761 p.

7. Orowan, E. and Scott, J.W., "The Creep of Metals," Journal of Iron and Steel Institute, Vol. 54, 1946, p. 45.

8. Ponter, A.R.S. et al., "The Force Exerted by a Moving Ice Sheet on an Offshore Structure: Part I The Creep Mode," Cold Regions Science and Technology, Vol. 8, 1983, pp. 109-118.

9. Vivatrat, V., Chen, V., and Bruen, F.J., "Ice Load Prediction for Arctic Nearshore Zone," Brian Watt Associates, Inc., Texas, 1984, 26p.

10. Wang, Y.S., "Rate-Dependent Stress-Strain Relationship for Sea Ice," First International Symposium on Offshore Mechanics and Arctic Engineering, New Orleans, LA, 1982, pp. 243-248.